Chemistry & Biology
Article

Regulation of the ROS Response Dynamics and Organization to PDGF Motile Stimuli Revealed by Single Nanoparticle Imaging

Cedric I. Bouzigues,[1,*] Thanh-Liêm Nguyên,[1] Rivo Ramodiharilafy,[1] Amy Claeson,[1] Pierre-Louis Tharaux,[2] and Antigoni Alexandrou[1]
[1]Laboratoire d'Optique et Biosciences, Ecole Polytechnique Université Paris Saclay, Inserm U696, CNRS 7645, 91128 Palaiseau, France
[2]Paris Cardiovascular Research Center, Inserm U 970, 75015 Paris, France
*Correspondence: cedric.bouzigues@polytechnique.edu
http://dx.doi.org/10.1016/j.chembiol.2014.02.020

SUMMARY

Although reactive oxygen species (ROS) are better known for their harmful effects, more recently, H_2O_2, one of the ROS, was also found to act as a secondary messenger. However, details of spatiotemporal organization of specific signaling pathways that H_2O_2 is involved in are currently missing. Here, we use single nanoparticle imaging to measure the local H_2O_2 concentration and reveal regulation of the ROS response dynamics and organization to platelet-derived growth factor (PDGF) signaling. We demonstrate that H_2O_2 production is controlled by PDGFR kinase activity and EGFR transactivation, requires a persistent stimulation, and is regulated by membrane receptor diffusion. This temporal filtering is impaired in cancer cells, which may determine their pathological migration. H_2O_2 subcellular mapping reveals that an external PDGF gradient induces an amplification-free asymmetric H_2O_2 concentration profile. These results support a general model for the control of signal transduction based only on membrane receptor diffusion and second messenger degradation.

INTRODUCTION

The organization in space and time of signaling pathways is an important element of signal processing and cell response formation. Reactive oxygen species (ROS) such as H_2O_2 are second messengers in numerous systems (Bedard and Krause, 2007; Kamata et al., 2005; D'Autréaux and Toledano, 2007; Rhee, 2006; Owusu-Ansah and Banerjee, 2009) and are implicated in migration either in normal situations (Grotendorst et al., 1982; Andrae et al., 2008), such as reparation of vascular lesions (Grotendorst et al., 1982; Andrae et al., 2008; Myllärniemi et al., 1999), or in fibrotic (Andrae et al., 2008) or tumoral contexts (Anastasiou et al., 2011; Andrae et al., 2008; Dhar et al., 2010; Abouantoun and MacDonald, 2009). The ability of second messengers to transduce asymmetric extracellular signals to trigger oriented cell motililty is a fundamental question. Although this question has been addressed in the case of Ca^{2+} signaling (Henley et al., 2004; Bouzigues et al., 2007), no data are available for the spatiotemporal organization of ROS signaling. The local ROS concentration results from the interplay of (1) production by NADPH oxidase (NOx) proteins following complex mechanisms (Bedard and Krause, 2007); (2) degradation by specialized enzymes or consumption for signaling purposes (Rhee, 2006); and (3) diffusion in the cytoplasm, according to an undetermined balance.

Vascular smooth muscle cells (VSMCs) respond to endothelin-1 (ET-1) and platelet-derived growth factor (PDGF) activating their respective receptors ET_A and PDGF receptor (PDGFR), respectively, by contraction (Turner et al., 1989) or by proliferation and migration (Andrae et al., 2008). These responses are, in both cases, mediated by the production of intracellular H_2O_2 (Daou and Srivastava, 2004; Kreuzer et al., 2003; Sundaresan et al., 1995; Banes-Berceli et al., 2005). We focused on PDGF pathway—a powerful chemotactic growth factor not only for VSMCs but also for a number of tumoral cells (Heldin and Westermark, 1999; Okada et al., 2012; Weima et al., 1990; Hellberg et al., 2010)—for which no quantitative observations of intracellular H_2O_2 support a comparison between normal and tumoral phenotype. PDGF stimulation causes PDGFR dimerization (Heldin and Westermark, 1999), leading to NOx protein activation through complex mechanisms involving PDGFR kinase activity (Chen et al., 2007) or direct coupling to G proteins (Kreuzer et al., 2003). Moreover, the existence of crosstalks between different signaling pathways—i.e., the transactivation of a second pathway by the specific activation of a first signaling cascade—has been sporadically reported, notably between PDGFR and epidermal growth factor receptors (EGFRs), probably through heterodimerization (Saito et al., 2001). The contributions of transactivations to the total cell response and their role in the control of its dynamics have, however, not been documented.

Here, we used a method based on the imaging of rare-earth doped nanoparticles (Casanova et al., 2009) to probe quantitatively and dynamically the local H_2O_2 concentration. The luminescence of YVO_4:Eu nanoparticles is indeed modulated by the oxidant level, and its measurement provides a unique, quantitative, space- and time-resolved detection of intracellular H_2O_2 concentration (Casanova et al., 2009), in contrast to organic sensors such as dichlorofluorescein or boronate-based probes (Lippert et al., 2011), which are not reversible and do not provide

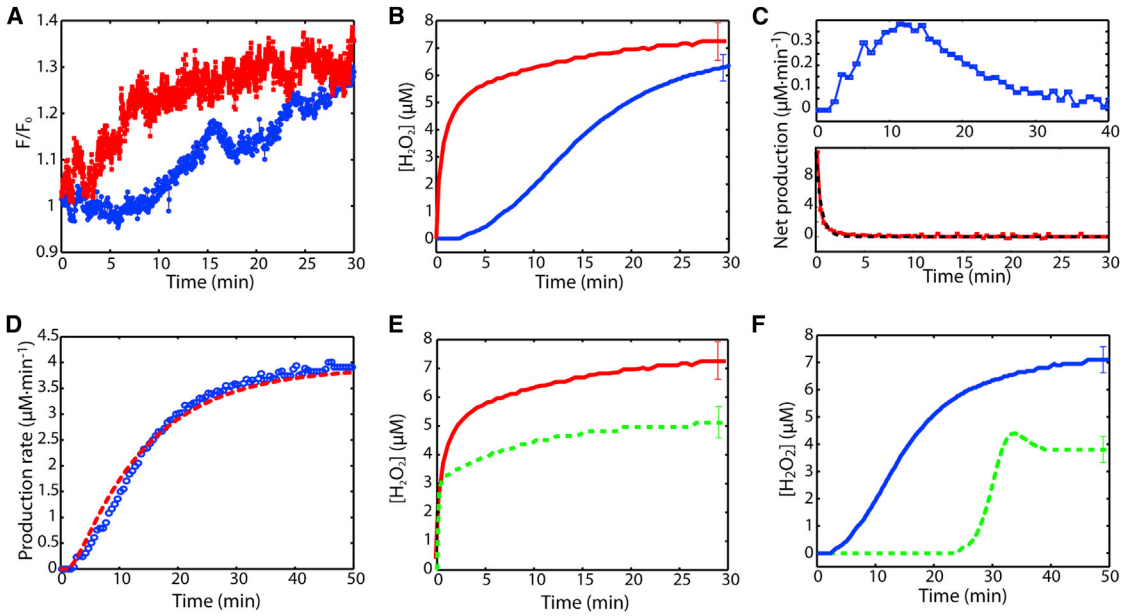

Figure 1. ROS Response in VSMCs

(A) Average luminescence F evolution normalized to the initial luminescence F_0 under saturating ET-1 (red dots, three cells) and PDGF (blue dots, five cells) stimulations.

(B) Evolution of the intracellular H_2O_2 concentration under the same conditions (ET-1 in red, PDGF in blue) determined from the signals in (A) according to Casanova et al. (2009) and Experimental Procedures.

(C) Net production of ROS under PDGF (top) and ET-1 (bottom; experimental data [red plain line] and exponential fit [blue dashed line]) stimulations.

(D) Instantaneous production of ROS under PDGF stimulation (blue circles) compared to the prediction by a diffusion-limited activation model (red dashed line) with a diffusion coefficient of $D = 0.11\ \mu m^2 \cdot s^{-1}$ and receptor density $\rho = 1.2\ \mu m^{-2}$ (Supplemental Information).

(E and F) Evolution of H_2O_2 concentration under stimulation with ET-1 in (E) and PDGF in (F), with inhibition of EGFR by AG1478 (green dashed line) compared to control (red line and blue line, respectively).

Error bars in (B), (E), and (F) indicate the SEM of the final ROS concentration as discussed in Results.

time resolution, and in contrast to genetically encoded sensors (Belousov et al., 2006), which have a limited dynamic range and may require ratiometric methods (Bilan et al., 2013) to obtain reliable measurements. Moreover, the nanoparticle consumption of H_2O_2 in the cell is negligible (Supplemental Information available online). Due to their size, they could possibly introduce perturbations to the cell physiology, but no such effect has been observed so far. These nanoparticles are not specific H_2O_2 sensors: however, we detected only H_2O_2 in cells as demonstrated by several control experiments, notably NOx and NO-synthase inhibitions (Supplemental Information; Figure S2) (Casanova et al., 2009). Complementary approaches based on carbon nanotubes measure the H_2O_2 efflux (Kim et al., 2011; Jin et al., 2010). However, the detection of intracellular H_2O_2 concentrations is the most relevant for the determination of the cell response, which led us to use single internalized nanoparticle imaging to investigate spatiotemporal patterns of ROS production.

RESULTS

Response to PDGF and ET-1

By imaging $Y_{0.6}Eu_{0.4}VO_4$ nanoparticles internalized in VSMCs stimulated by saturating concentrations (Graves et al., 1996; Wiley and Davenport, 2004) of the PDGF BB isoform (PDGF-BB) (100 ng/ml^{-1}; i.e., 4 nM) or of ET-1 (270 nM), we quantitatively compare the oxidant response to each kind of stimulus (Figures 1A and 1B). The method for obtaining absolute H_2O_2 concentrations from luminescence measurements is described briefly in Experimental Procedures and in our previous work (Casanova et al., 2009). Although this method is not H_2O_2 specific, we exclusively detect ROS under the H_2O_2 form in these experiments, as explained in the Supplemental Information (Casanova et al., 2009). We measure the H_2O_2 concentration by averaging the luminescence signal for typically five to ten nanoparticles in each cell. We then independently repeat the experiment three to five times with different cell cultures and average the nanoparticle signal for the different cells. Unless indicated otherwise, the number of cells for each condition is the number of independent single cell experiments. We then obtain the average H_2O_2 concentration as explained in Experimental Procedures and in the Supplemental Information (Figures S1 and S2) (Casanova et al., 2009). In the whole article, the indicated error for the average ROS concentration is the SEM resulting from single nanoparticle variability inside each cell (see Supplemental Information and Figures S1 and S4) and intercellular dispersion (Figure S1) and is dominated by the latter.

The intracellular H_2O_2 concentration in steady state after a continuous stimulation is comparable: 7.4 ± 0.7 μM (three cells) for ET-1 and 7.1 ± 0.5 μM (five cells) for PDGF, with no significant intracellular variability detected by different nanoparticles in the cytosol (Figure S4), as reported elsewhere (Casanova et al.,

2009). However, the dynamics of the concentration increase are significantly different: whereas the H_2O_2 concentration rises immediately after applying the ET-1 stimulation with a characteristic time (see Experimental Procedures), $T_{ET\text{-}1} = 2.1 \pm 0.6$ min, the buildup of the response under PDGF stimulation requires over 10 min ($T_{PDGF} = 14.8 \pm 0.5$ min) (Figures 1A and 1B). This reveals different mechanisms for ROS production in the activation of the receptors and/or of NOx proteins. The measured concentration at a given time thus results from the fine tuning between receptor and/or NOx activation and effective deactivation due to receptor endocytosis after stimulation (Pahara et al., 2010) and H_2O_2 diffusion and degradation (Rhee, 2006).

H_2O_2 Production Rate

In the case of ET-1, the H_2O_2 elevation rate—i.e., the ROS concentration elevation per time unit $d[H_2O_2]/dt$ under a constant stimulation—is maximal at the beginning of the stimulation and constantly decreases with time (Figure 1C, bottom). This behavior can be explained by a model in which the ROS concentration temporal profile is the balance between a constant H_2O_2 production rate, $S_{ET\ -\ 1}$, and degradation with a first-order kinetics:

$$\frac{d[H_2O_2]}{dt} = S_{ET-1} - k_{ET-1}[H_2O_2].$$

This model predicts a simple exponential response and is in good agreement with our experimental data. Fitting the experimental data with this model (Figure 1C, bottom, dashed green line) yields a production rate, $S_{ET\ -\ 1} = 2.4 \pm 0.6\ \mu M \cdot min^{-1}$, and a degradation rate, $k_{ET\ -\ 1} = 0.33 \pm 0.1\ min^{-1}$, consistent with a moderate peroxiredoxin (Kang et al., 1998) or catalase-like activity (Beers and Sizer, 1952). A constant ROS production rate, stable immediately after the beginning of stimulation, reveals a fast activation of NOx proteins. This might be due to the facilitated activation of receptors and NOx colocalized in microdomains as reported for angiotensin signaling (Zuo et al., 2005).

In the case of PDGF stimulation, the H_2O_2 elevation rate $d[H_2O_2]/dt$ at first increases and peaks after about 15 min of stimulation to finally decrease (Figure 1C, top). This reveals a slow reorganization either of the ligand detection system or of the ROS production system followed (>10 min) by the progressive deactivation of the system due either to an increasing degradation of ROS or to receptor inactivation and/or internalization. By assuming that the degradation depends only on ROS concentration and not on the production pathway, and is thus the same for ET-1 and PDGF stimulation, we obtained

$$\frac{d[H_2O_2]}{dt} = S_{PDGF}(t) - k_{ET-1}[H_2O_2],$$

where $S_{PDGF}(t)$ is the time-dependent ROS production. By solving this equation through standard computations (see Supplemental Information), we determined the instantaneous H_2O_2 production rate $S_{PDGF}(t)$ in the case of PDGF stimulation (Figure 1D, blue circles). This reveals the progressive buildup of the oxidant response with a persistent production in the time range of our experiments.

Without excluding other regulation pathways such as modulation of peroxiredoxin-like activity, we quantitatively account for this progressive buildup (Figure 1D) by hypothesizing that the ROS response is determined by a diffusion-limited dimerization of free receptors described by a numerical model presented in the Supplemental Information. Fitting our experimental data with this model, we obtain a diffusion coefficient of $D = 0.11\ \mu m^2 \cdot s^{-1}$ (Figure 1D, red curve), which is reasonable for a freely diffusing membrane protein (Edidin et al., 1994; Bouzigues and Dahan, 2007; Kusumi et al., 2005; Ljungquist-Höddelius et al., 1991). The exact obtained value depends on our hypothesis of a stimulation-independent ROS degradation rate. However, a different rate after PDGF stimulation would not qualitatively affect our conclusion concerning the control of the ROS production kinetics by membrane receptor diffusion.

Our model is thus reasonable to account for the experimental data: the balance between diffusion-limited activation of PDGFRs, $S_{PDGF}(t)$, is sufficient to explain the observed oxidant response kinetics. This indicates that the kinetics of the oxidant response saturation may not be controlled by receptor inactivation or recycling but by ROS degradation only. This would imply that both receptor recycling and NOx inactivation occur at longer time scales (>30 min).

EGFR Transactivation

Transactivation of EGFRs with specific mechanisms has been reported under stimulations by G protein-coupled receptors, such as ET_A (Chansel et al., 2006), or receptor tyrosine kinases (RTKs), such as PDGFR (Saito et al., 2001). By application of a specific EGFR kinase inhibitor (AG1478; see Experimental Procedures), we probe the modifications of the ROS production under stimulation by ET-1 or PDGF. In both cases, we observed a decrease of the ROS concentration in the steady state down to $5.4 \pm 0.6\ \mu M$ and $3.8 \pm 0.5\ \mu M$ for ET-1 and PDGF stimulation, respectively (Figures 1E and 1F, respectively, for n = 3 and 5 independent experiments). This demonstrates transactivation of EGFRs, whose inhibition diminishes, respectively, by 26% ± 15% and 44% ± 10% the total response to ET-1 and PDGF stimulations.

In the case of ET-1 stimulation, the initial dynamics of the response after EGFR inhibition is unchanged (Figure 1E), with a decreased sensitivity. This reveals that the initial event leading to ROS production is the direct NOx activation by ET-1 receptors. In the case of PDGF stimulation, however, the H_2O_2 production after EGFR inhibition is dramatically slowed down ($T_{PDGF} = 29.1 \pm 0.4$ min; Figure 1F), which indicates that EGFR transactivation is the first event leading to ROS production. Since mechanisms of heterodimerization have been proposed for the crosstalk between EGFR and PDGFR (Saito et al., 2001), we can assume that the response timing is controlled by the density and the diffusion dynamics of the receptors at the cell membrane. In addition, the inhibition of EGFR kinase causes a depletion of the available receptor pool (EGFR and PDGFR) by forming inactive heterodimers and consequently slowing down the response. This is consistent with results obtained for epidermal growth factor (EGF) signaling, in which EGFR inhibition by AG1478 results in the formation of inactive dimers (Gan et al., 2007). The faster EGFR-dependent ROS production on PDGF stimulation might furthermore be due to a different organization at the membrane of PDGFRs and EGFRs, leading to a facilitated NOx activation by EGFRs.

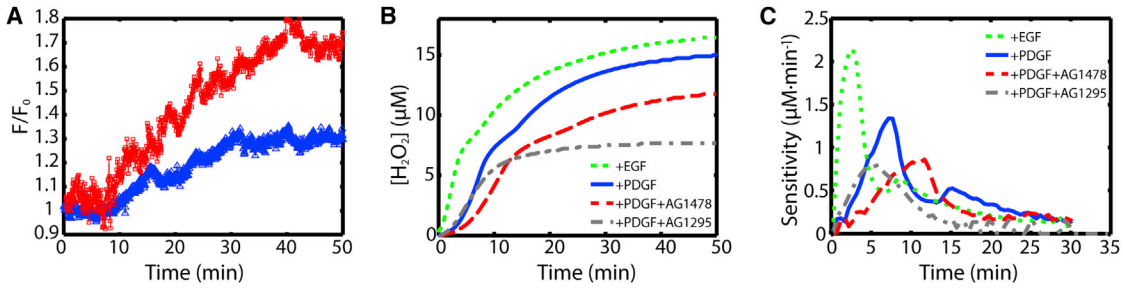

Figure 2. ROS Response in HeLa Cells

(A) Average luminescence F evolution normalized to the initial luminescence F_0 during a 100 ng/ml PDGF stimulation in VSMCs (blue triangles, five cells) and HeLa cells (red squares, five cells).

(B) Concentration of H_2O_2 in HeLa cells under EGF (green dots) or PDGF stimulation without further treatment (blue line) or combined with treatment by AG1478 for EGFR inhibition (red dashed line) or AG1295 for PDGFR inhibition (gray dashed line).

(C) Net production of ROS under EGF (green dots), PDGF without (blue line) and with AG1478 (red dashed line) or AG1295 (gray dashed line).

H_2O_2 Response in HeLa Cells

We then probed the response to PDGF (Figure 2A) in tumoral HeLa cells (coming from a biopsy of a cervical tumor) known to constitutively express PDGFRs (Woo et al., 2007; Fukumoto et al., 2011). As in VSMCs, we observed a saturating elevation of ROS concentration (Figure 2B), with a peak in sensitivity after a few minutes (Figure 2C). However, consistently with the high PDGFR expression observed in cervical tumors (Mayer et al., 2000), the intracellular H_2O_2 concentration in the steady state under PDGF stimulation is significantly higher ($p < 0.01$, Kolmogorov-Smirnov test [KS test]): 16.1 ± 0.5 μM, and this response is faster (T = 11.9 ± 0.5 min). EGFR inhibition with AG1478 slows down the response significantly (T = 14.0 ± 0.8 min) but less dramatically than in normal VSMCs. The response to a saturating EGF concentration appears to be even faster (T = 8.4 ± 0.4 min). Inhibition of PDGFR kinase activity by AG1295 (Kovalenko et al., 1994) causes a 52% ± 5% lower response after 50 min without change at short times (Figure 2B), which clearly displays that PDGFR kinase activity contributes to the ROS production. EGFR activation is thus PDGFR kinase activity independent, which indicates that EGFR transactivation occurs at an initial step of signal transduction. Altogether, these elements point to a similar ROS production mechanism in tumoral and normal cells, causing a delay before ROS production after stimulation (Figure 2C), with kinetics determined by the diffusion-limited receptor homo- and heterodimerization. The fast kinetics in HeLa cells can be explained by the high PDGFR expression in cervical tumors (Mayer et al., 2000). The relative receptor density at the membrane may thus be a regulation element of the ROS response kinetics.

Dependence on PDGF Concentration

To further probe the control of ROS response, we performed PGDF-BB stimulation in HeLa cells at subsaturating concentrations. A significant response was detected between 2 and 100 ng • ml^{-1} (Figure 3A). By observing the dependence of the steady-state response to stimulus concentration (Figure 3A), we measured the effective dissociation constant—i.e., the PDGF concentration required to obtain half of the maximal ROS response—of the PDGF detection system, K_D = 4.2 ± 0.4 ng • ml^{-1}. The Hill coefficient close to 1 (n = 1.4 ± 0.2) obtained by fitting the response with the Hill equation (Figure 3A) indicates the absence of cooperativity in the PDGF-dependent ROS production. Moreover, the response kinetics is independent of the external PDGF concentration (Figure 3B). This reveals that the delayed ROS production is not due to the biochemical properties of the interactions in the cascade; i.e., the delayed ROS production is not due to a nonlinearity in the reaction scheme leading from PDGFR activation to ROS production. If that were the case, a change in the ligand concentration would affect the reaction rates, which is not what we observed. The control of the response is thus more likely due to a spatial reorganization of the transduction pathway, such as diffusion-limited receptor dimerization, as suggested earlier.

It has been reported that the organization of membrane receptors and NOx proteins in microdomains regulate the ROS production, notably in the case of EGFR transactivation after angiotensin stimulation (Clempus and Griendling, 2006; Zuo et al., 2005). More generally, the recruitment of RTK receptors in microdomains is furthermore essential for the regulation of their signaling pathways (Irwin et al., 2011). In order to test whether any such effect was involved in PDGFR activation and ROS dynamics production, we tracked single fluorescent nanocrystal (QDot)-labeled PDGFRs in the membrane of HeLa cells and revealed that they were freely diffusing both with and without stimulation (C.I.B., R.R., and A.A., unpublished data). This demonstrates that they are not organized in microdomains, neither spontaneously prior to stimulation nor after PDGF stimulation. This fact supports our model of PDGFR activation being limited by freely diffusing receptor dimerization.

Asymmetric PDGF Stimulation

Under asymmetric PDGF stimulations, i.e., external PDGF concentration profiles in which the concentration is different at opposite extremities of the cell, different cell types are able to migrate by chemotaxis toward a PDGF source (Grotendorst et al., 1982; Seppä et al., 1982). An intracellular gradient of second messenger, therefore, has to be maintained for durations longer than several minutes to induce migration. However, the spatial organization of ROS inside the cytoplasm has not been measured so far. In cells submitted to a homogeneous PDGF stimulation, the ROS local concentration does not depend on

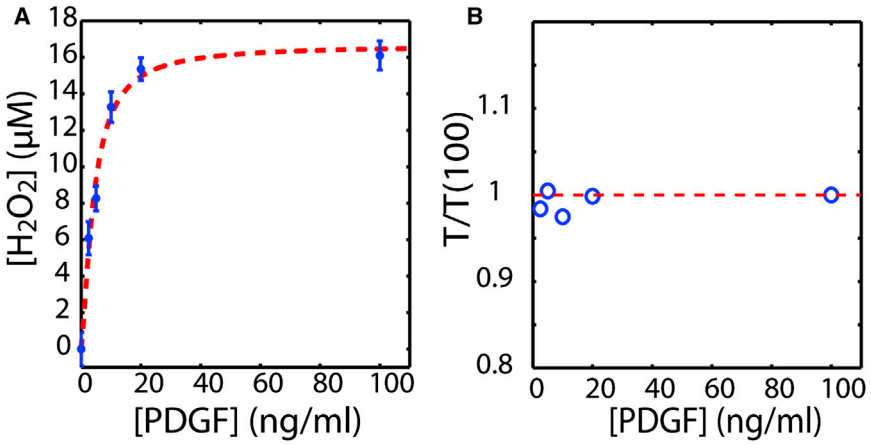

Figure 3. Dose Dependence of the Oxidant Response to PDGF

(A) H_2O_2 concentration after 50 min of PDGF stimulation of HeLa cells (blue dots) fitted by the Hill equation

$$[H_2O_2] = A \cdot \frac{[PDGF]^n}{[PDGF]^n + K_D^n}$$

(red dashed line, A = 16.7 μM, KD = 4.2 ng · ml^{-1}, n = 1.4).

(B) Characteristic time *T* (resulting from the fit with a function $A(t^n/(t^n + T^n))$ of the intracellular ROS increase for different PDGF concentrations compared to T(100) the characteristic time observed for [PDGF] = 100 ng · ml^{-1}. All concentrations were tested on five different cells during five independent experiments, and the average signal of these five cells was analyzed (approximately five to ten nanoparticles per cell). Error bars indicate SEM.

the position inside the cell according to an identified pattern with an intracellular variation inferior to 1 μM (Casanova et al., 2009) (Figure S4). This implies that ROS are not trapped in specific compartments but more likely diffuse—freely or not—in the cytoplasm.

We then cultured HeLa cells for several days in T-shaped microchannels, through which PDGF-controlled gradients, able to trigger migration in the direction of high PDGF concentration after 2 hr at ~5 μm · hr^{-1} (three independent experiments in glucose-rich medium; Experimental Procedures), were created (Figures 4A and 4B; Experimental Procedures). In contrast, the stimulation by a homogeneous PDGF concentration was unable to induce migration (Experimental Procedures). We imaged internalized nanoparticles during 30 min with a spatial ~30 nm accuracy (Figure 4B) to measure the local ROS concentration inside these cells submitted to a PDGF gradient of controlled shape (Experimental Procedures). The location of the observed cells was chosen in such a way that the PDGF concentration between the two sides of the cell varies from 0 to ~10 ng · ml^{-1}. In our conditions, shear stress is sufficiently low to elicit no ROS response (Figure S3). During all nanoparticle imaging experiments led in Hank's balanced salt solution (HBSS)-HEPES buffer, cells remain static in the gradient, with an average displacement less than 1 μm.

Under this asymmetric stimulation, we revealed significant anisotropies in the ROS intracellular concentration by comparing the average concentration in the proximal part of the cells (side exposed to high PDGF concentration) to that in their distal part (exposed to low concentration, $p < 0.01$, KS test) (Figure 4C), in contrast to cells stimulated by a homogeneous PDGF bath, where no significant anisotropies were detected (Figure S4). Under continuous stimulation, an asymmetry in intracellular H_2O_2 concentration is thus maintained within the cell. We moreover determined the local concentration as a function of the absolute position (see Experimental Procedures) in the PDGF gradient after 30 min stimulation (Figure 4D). We observed a direct correspondence between the local PDGF concentration and the local intracellular H_2O_2 concentration. As expected from our homogeneous stimulation experiments (Figure 3B), no difference in the kinetics of ROS production was observed. The cell thus produces a mapping of the external stimulus in the cytoplasm (Figure 4D) by maintaining a local H_2O_2 concentration proportional to the local stimulation. This demonstrates the absence of amplification processes between PDGFR activation and ROS production and the existence of mechanisms maintaining ROS asymmetries in the cytoplasm despite the diffusion-induced homogenization.

DISCUSSION

Our results provide an insight into the dynamics of the oxidant response formation and lead us to propose mechanisms for its kinetics and the maintenance of intracellular spatial patterns induced by chemical cues.

First, different stimulations can cause the production of the same second messenger (ROS) but with a specific dynamics, which may determine specific physiological responses.

Second, we revealed that transactivation of EGFR is the initial event in the PDGF signaling cascade. The difference in transactivation dynamics are likely due to the different transactivation mechanisms through heterodimerization for PDGF (Saito et al., 2001) and through cleavage of heparin-binding EGF for ET-1 stimulation (Chansel et al., 2006). Our results show that EGFR transactivation is used by the cell for the regulation of both the quantity and kinetics of ROS production. The control of this process—for instance, through the tuning of receptor density at the membrane—might determine the nature of the cell response in an in vivo context with simultaneous multiple stimulations. The production of specific messengers in the cell but, equally important, the temporal profiles of this production are thus likely to shape the cell response specificity.

Third, we demonstrated delayed cell sensitivity to PDGF, compared to an ET-1-induced response that is PDGF concentration independent and is likely related to a spatial reorganization of the signaling cascade. This could constitute an intrinsic method of temporal filtering for the cell: the requirement of a continuous stimulation to enhance the cell sensitivity could be a way to eliminate the contribution of transient stimuli. This property should be of major physiological interest for migrating cells to increase the robustness of chemotaxis—i.e., its

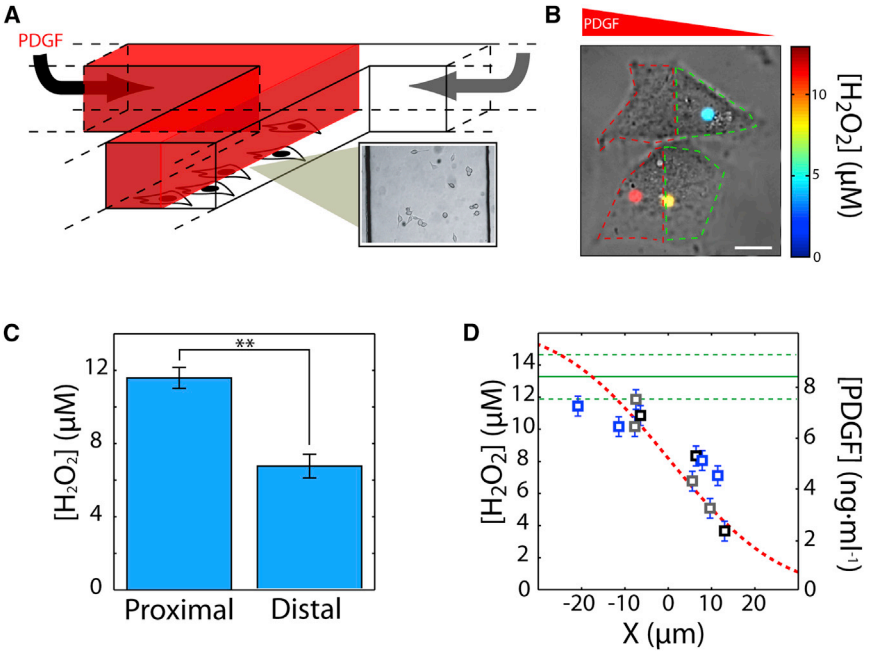

Figure 4. ROS Production on Asymmetric PDGF Stimulation

(A) Schematic of the microfluidic stimulation system. Cells are plated in the center branch of the T, while observation medium with or without PDGF (10 ng • ml^{-1}) is injected through the right and left branches, respectively, with the same flow rate. Inset: image of HeLa cells in a 500-μm-wide channel. The asymmetric stimulation is created by the PDGF diffusion profile around the T axis.

(B) Image of three nanoparticles in two cells submitted to a gradient of PDGF (PDGF concentration decreases from left to right). The center axis of the channel lies in the middle of the image. Scale bar, 10 μm. Distal and proximal parts are indicated by green and red dashed lines, respectively.

(C) Average H_2O_2 concentration (four cells in three independent experiments) in the half of the cell closest (proximal) or furthest (distal) of the PDGF source (11 nanoparticles, $p < 0.01$, KS test). Error bars indicate SEM. The two halves are determined by the median axis of a manually drawn polygon around each cell with a custom made Matlab interface.

(D) H_2O_2 concentration (four cells in three independent experiments, 11 nanoparticles) as a function of the position in the gradient (blue, gray, and black squares, each color representing an independent experiment). The center of the channel is indicated by "0." The error bars indicate the uncertainty in H_2O_2 concentration determination due to internanoparticle variability (Experimental Procedures) (Casanova et al., 2009). The absence of nanoparticles in the center is due to the presence of the nucleus. The red dashed curve is the concentration profile of PDGF due to pure diffusion at the interface $(C_0/2)\mathrm{erfc}(x/\sqrt{2Dt})$ estimated for $C_0 = 10$ ng • ml^{-1} and $t = 3$ s—i.e., the time taken by the flow to reach the selected cell (see Experimental Procedures)—and for a diffusion coefficient of DPDGF = 100 $\mu m^2 \cdot s^{-1}$ typically expected for a 25 kDa protein as PDGF-BB in water. Average concentration measured for a homogeneous stimulation ([PDGF] = 10 ng • ml^{-1}, green plain line) with the SD (green dashed line) of this measurement due to the dispersion of signals detected for single nanoparticles resulting from inter- and intracellular dispersion of the response to PDGF.

See also Figure S4.

resistance to undesired migration due to transient external signals—as reported in different systems (Bouzigues et al., 2010; Dehmelt and Bastiaens, 2010). The difference between ET-1 and PDGF pathways is thus probably related to their physiological function: while ET-1 triggers contraction acting at the single cell level, the PDGF-induced migration needs to be tightly controlled to avoid any undesired effect to the whole organ or organism. The difference between VSMCs and tumoral HeLa cells seems essential in this context: the faster response of HeLa cells implies a degraded temporal filtering and, consequently, a facilitated migration typical of metastatic cells. The relative level of expression of EGFRs and PDGFRs at the membrane and their diffusive properties could be the key for the control of this phenomenon by modulating the cell sensitivity to chemotactic gradients. Although HeLa cells are only a particular example of tumoral cells, this impaired cell response timing might provide a clue to understand metastatic transition.

By considering (1) the response kinetics independence of PDGF concentration (Figure 3B); (2) the dynamics difference between ET-1 and PDGF pathways, with a delay before ROS production in the case of PDGF, indicating their regulation by the first steps of the transduction cascade, i.e., the receptor activation; and (3) the shorter response time in tumoral HeLa cells, which likely have higher receptor density levels, we propose that the ligand-induced diffusion-limited PDGFR homo- and/or heterodimerization (Figure 1D; Supplemental Information) should be the limiting step for the dynamics of the ROS production in the PDGF pathway. The timing for ROS production would thus be determined by the time required for diffusive search for interaction of two EGFR or PDGFR monomers. We cannot completely exclude that this timing could be due to the NOx activation process. However, the kinetics difference between ET-1 and PDGF signaling, which both involve EGFR transactivation, suggests that the observed delay before ROS production after PDGF stimulation is due to the dynamics of the first steps of the signaling cascade. This strongly supports our hypothesis that PDGFR/EGFR activation is the limiting step in PDGF signaling.

The regulation properties of intracellular biochemical networks—and, notably, their temporal integration capacities—are essential for the cell physiological response and can be based either on the topology of the interaction networks or on spatial reorganization of the receptors involved (Kinkhabwala and Bastiaens, 2010). Here, we propose a general mechanism, where the membrane dynamics of the receptors is the process responsible for the control of second messenger production. The main control parameter is thus the receptor density, creating either an intrinsic temporal filtering at low membrane density or an accelerated response in cells with high receptor expression levels.

Finally, we present a demonstration of the existence of a persistent intracellular H_2O_2 gradient linearly matching the external PDGF migration-triggering gradient (Figure 4D). This internal gradient is only observed in cells subjected to a PDGF gradient that causes migration, which indicates that the

formation of a ROS asymmetric profile is physiologically essential to trigger the migration response.

This profile could result only from the degradation and diffusion balance of PDGF-induced ROS, but it could also be from the combination of the contributions of multiple pathways activated during migration. It has notably been reported that ROS production and integrin activation were tightly coupled in migrating cells (San Martín and Griendling, 2010). Moreover, it was shown that mechanical changes could activate ROS through focal adhesion points or integrins (San Martín and Griendling, 2010; Koller, 2002; Lin et al., 2013) acting as mechanosensors. However, we observed no ROS production due to mechanical stimulation only (Figure S3), and our observations take place at early times, before any remodeling leading to migration. Furthermore, the ROS concentration observed in the region of high PDGF concentration (10 ng $\cdot$ ml^{-1}) in the gradient is similar to the measured concentration for a homogeneous stimulation with the same concentration. These elements indicate that, although integrin-induced ROS production cannot be formally excluded, it does not contribute significantly to our observations. On the other hand, integrins have been reported as a target of H_2O_2 (de Rezende et al., 2012), which may thus be quickly consumed when a migration-inducing PDGF signal is applied. This fact could contribute to the shape of the observed internal gradient, as explained later.

The asymmetric ROS profile we measured is consistent with a model assuming (1) local ROS production varying linearly with the external PDGF concentration (2), free diffusion of H_2O_2 in the cytoplasm, and (3) degradation proportional to [H_2O_2] (Supplemental Information). The amplitude of the internal gradient is thus determined by the ratio between the degradation kinetics constant, k, and the ROS diffusion coefficient, D_{ROS} (Supplemental Information). The absence of attenuation in the translation (Figure 4D) of the external signal into ROS concentration in the cytoplasm indicates that HeLa cells operate in a regime where degradation is faster than diffusion.

Qualitatively, the persistence of an intracellular gradient indicates that ROS degradation is a fast process compared to their diffusion, in order to maintain a profile matching the PDGFR activation profile by external PDGF. We can model this effect through a simple reaction-diffusion equation (Supplemental Information). If we assume that ROS degradation is mostly stimulation and cell independent and use the experimentally determined value of the ROS degradation rate, k, for VSMCs under ET-1 stimulation, we find that D_{ROS} should be $<10\ \mu m^2 \cdot s^{-1}$ (Supplemental Information). This result indicates either the existence of mechanisms hindering H_2O_2 diffusion in the cytoplasm, possibly due to the presence of scavengers or transient interactions with molecular partners, or that the ROS degradation pathway is modified in HeLa cells, leading to a fast ROS degradation. This second mechanism could result from peroxiredoxin upregulation, which was observed in some cervical tumors (Kim et al., 2009), or from an increased ROS consumption in migration controlling pathways.

Our measurements indicate the existence of a functional asymmetric ROS production, but the physiological role of the cytosolic H_2O_2 gradient remains unclear. It is indeed unknown if this gradient directly controls effector activation or if it only reflects an asymmetric signaling located in subdomains at the cell membrane. Although our results indicate that PDGFRs are not confined in microdomains in our system, it has indeed been revealed that membrane-associated peroxiredoxins may be inactivated by phosphorylation due to PDGF or EGF stimulation and thus cause a local H_2O_2 accumulation in the vicinity of membrane subdomains (Woo et al., 2010). This has led to the hypothesis that signaling, notably, protein tyrosine phosphatase (PTP) oxidation, occurs only at membrane-associated signaling sites.

Although transient association of PTPs with PDGFRs has been demonstrated (Meng et al., 2002), the localization of H_2O_2-targeted PTPs has not been shown to be exclusively associated to membrane microdomains. In particular, microtubule association of PTPs has been shown to be regulated by EGFR activation (Sines et al., 2007). In addition, micromolar concentrations of H_2O_2, comparable to the cytosolic concentration detected in our experiments, are known to inactivate PTPs (Denu and Tanner, 1998). Moreover, we argue that fast ROS degradation compared to ROS diffusion dynamics is essential to maintain a gradient likely to elicit a migration response. Therefore, it is unlikely that all signaling events occur in domains where peroxiredoxins and ROS degradation are inactivated, unless these domains are sparsely distributed and isolated from each other.

Compartmentalization of peroxiredoxin activity might thus contribute to shape the intracellular ROS profile and the response asymmetry, but cytosolic ROS profile is likely to be physiologically essential, notably for cytoskeleton-associated PTPs (Sines et al., 2007). More probably, the cell response is both regulated by signaling in high ROS concentration membrane-associated subdomains and by the cytosolic ROS concentration, resulting from signaling at the membrane. This is consistent with Ca^{2+}-controlled chemotaxis systems in which localized Ca^{2+} influxes contribute to shape a cytosolic gradient that regulates the migration response (Henley et al., 2004; Bouzigues et al., 2007).

In most chemotactic systems, the enhancement of reliability and sensitivity relies on local (asymmetric) excitation/global inhibition mechanisms (Iglesias and Devreotes, 2008; Franca-Koh and Devreotes, 2004). In these systems, the external gradient is amplified due to the fact that only regions where the stimulation is high can produce a sufficient quantity of second messenger to overcome the inhibition acting on the whole cell. The model we propose here differs by assuming a degradation rate proportional to the local ROS concentration and a linear response to receptor activation, which leads to the absence of amplification in contrast with other chemotactic systems (Bouzigues et al., 2007; Ueda et al., 2001; Servant et al., 2000). The gradient persistence is thus only the result of the balance between intracellular diffusion, which tends to homogenize intracellular ROS concentration, and degradation, which leads the ROS concentration to follow the activation profile. This system has thus analogies with the model developed to explain the polarization of budding yeast expressing activated Cdc42, where the balance between endocytosis and membrane diffusion regulates cortical polarity in a similar way (Marco et al., 2007; Slaughter et al., 2009).

SIGNIFICANCE

Altogether, these results support the hypothesis that the formation and maintenance of a second-messenger (ROS)

concentration profile is controlled by a three-step mechanism: (1) activation, (2) intracellular diffusion, and (3) degradation. The activation step differs notably with the type of stimulation, and its kinetics is determined by the properties of membrane receptors. It provides either temporal filtering of the external signal due to slow diffusion limited dimerization, in the case of PDGF, or a direct transduction in the case of ET-1.

The balance between diffusion and degradation is responsible for the shape of the internal gradient (Postma and Van Haastert, 2001). The tuning of these processes (by modulation of the receptor expression or of the degradation enzyme activity, for example) may thus be sufficient to produce different ROS spatiotemporal patterns to adjust the cell response in physiological or pathological contexts and may constitute an efficient mechanism of dynamic adaptation.

From a methodological point of view, we developed methods that simultaneously control the local chemical environment and locally probe intracellular chemical reactions controlling the cell response by the combination of microfluidics and single nanoparticle imaging. This approach is general and may be applied to the numerous systems in which ROS signaling is involved and become a central tool to dissect pathways with spatial and temporal resolution. Based on these results, we propose an added insight into the spatiotemporal regulation of intracellular ROS concentration by revealing the mechanisms controlling H_2O_2 kinetics and intracellular localization in the PDGF pathway. Although we demonstrated these features in the specific case of PDGF, these results are likely to have broader implications in cell signaling and constitute a framework for the dynamic building of subcellular responses.

EXPERIMENTAL PROCEDURES

Cell Culture

VSMCs were isolated from collagenase-treated aortas of male C57BL6 mice (10–14 weeks old). HeLa cells and VSMCs were cultured in Dulbecco's modified Eagle's medium (Invitrogen) and RPMI medium (Invitrogen) respectively, supplemented with 10% and 20% fetal calf serum, respectively, at 37°C in an atmosphere containing 5% CO_2. Cells were plated on glass coverslips 48 hr (HeLa) or 72 hr (VSMCs) prior to experiments and serum deprived overnight before experiments. All nanoparticle experiments were performed in HBSS-HEPES observation medium, pH = 7.4. EGFR and PDGFR phosphorylation inhibition were achieved, respectively, by treating cells for 30 min at 37°C with 500 nM AG1478 (Merck) or with 500 nM AG1295 (Merck) before experiments and then mounted in observation medium containing the same inhibitor concentration.

Imaging

For all experiments, $Y_{0.6}Eu_{0.4}VO_4$ nanoparticles synthesized as described elsewhere (Casanova et al., 2009) (Supplemental Information) were internalized by pinocytosis and photoreduced until a steady-state situation was reached, using an excitation intensity of 1.6 kW/cm^2 at 466 nm for 250 s and illuminated for 300 s at 0.3 kW/cm^2 without stimulation to ensure the stability of the luminescence. Oxidant detection was then performed (0.3 kW/cm^2, integration time = 2.8 s). As demonstrated elsewhere (Casanova et al., 2009), no additional lethality was induced by the presence of nanoparticles in the cytosol, and NOx inhibition by apocynin causes the absence of ROS production. We also checked with trypan blue labeling that a large majority of cells were unaffected by the full experimental sequence (nanoparticle photoreduction and subsequent observations) (Casanova et al., 2009).

H_2O_2 Concentration Determination

Determination of ROS concentration was performed as explained elsewhere (Casanova et al., 2009) (Supplemental Information; Figure S1). Briefly, we fitted the luminescence signal of intracellular single nanoparticle emission spots with a two-dimensional Gaussian to determine the total signal. The spatial resolution of these measurements is the localization accuracy of single nanoparticles; in our case, about 30–40 nm. The nanoparticles seem to be trapped in the dense cytosolic environment and move less than 1 μm during the whole experiment (Figure S1). Their signal thus reflects the ROS concentration at their specific location. Note that the steady-state H_2O_2 concentration before stimulation is on the order of 10^{-7} μM (D'Autréaux and Toledano, 2007), which is below our detection limit. We thus detected the concentration produced on external stimulation. For homogeneous stimulation, this signal does not vary significantly for different particles (Casanova et al., 2009) (Figure S1). The signal is averaged for typically five to ten nanoparticles in each cell and is then averaged for independent experiments on different (three to five) cells. Then, by using this average signal and its first temporal derivative, we computed through the calibration table presented in the Supplemental Information (Figure S1) (Casanova et al., 2009) the concentration profile as a function of time, which was then fitted by a saturating power law,

$$A\frac{t^n}{t^n + t_0^n},$$

to determine the characteristic time of the oxidant response for PDGF, or with an exponential for ET-1. We determined the H_2O_2 concentration with a typical 0.5 μM accuracy for a single nanoparticle (due to interparticle variability; Casanova et al., 2009) The error indicated in the text for the average response is thus mostly due to intercellular variations, which are typically of the order of 1 μM. As reported elsewhere (Casanova et al., 2009), no signal was detected in the absence of stimulation, and external H_2O_2 stimulation was efficiently detected by internalized nanoparticles. We have furthermore shown by several control measurements that the oxidant responsible for the luminescence signal recovery on PDGF or ET-1 stimulation is H_2O_2 in our experiments (Supplemental Information) (Casanova et al., 2009).

Microsystem Fabrication and Use

Master molds were made by lithography of UV-sensitive solid film (Eternal) and polydimethylsiloxane (PDMS) with 10% curing agent (Dow Corning) was poured in the mold and baked at 75°C for 1 hr. Microsystems (height, 50 μm; width, 1,000 μm) were sealed by bonding 30 s air-plasma-treated PDMS on a glass coverslip and then treated by air plasma for 1 min to ensure sterility and wettability. Cells at high concentration (10^6 cells per milliliter) were then injected in the microsytem, which was covered with culture medium. A permanent gradient on the T axis was created by injecting HBSS-HEPES in the first branch of the T junction and 10 ng • ml^{-1} PDGF in HBSS-HEPES in the second branch with the same flow rates. No significant motion of the cells was observed during the experiment duration in these conditions. However, cell migration was induced by such PDGF gradients in HEPES-buffered minimum essential medium (Sigma-Aldrich) supplemented with 6 g • l^{-1} glucose and 10% fetal calf serum. We estimated the cell displacement by positioning the center of the cell (defined by a manually drawn polygon on a custom Matlab interface) before and after 2 hr of stimulation and measured an average migration speed of ~5 μm • h^{-1} (ten cells, three independent experiments). Cells placed in similar conditions, but submitted to an identical 10 ng • ml^{-1} PDGF concentration in the two branches of the T junction, do not display any detectable oriented motion, i.e., present a displacement smaller than 1 μm (eight cells, three independent experiments). Cells for asymmetric ROS detection were chosen so that the approximate center of the cell is on the median axis of the channel about 2 mm after the T junction. In cases where selected cells are not at exactly 2 mm from the T junction, the flow rate was slightly adjusted so that the gradient on the cell was the same as expected 2 mm after the junction, with a flow rate of Q = 3 μl • min^{-1}, resulting in a typical shear stress of <0.1 pN/μm^2.

SUPPLEMENTAL INFORMATION

Supplemental Information includes Supplemental Experimental Procedures and four figures and can be found with this article online at http://dx.doi.org/10.1016/j.chembiol.2014.02.020.

ACKNOWLEDGMENTS

This work was funded by the Competence Centre in Nanosciences (C'Nano), Ile de France, and the RTRA Triangle de la Physique. We thank Markus Schoeffel, Geneviève Mialon, Thierry Gacoin, and Jean-Pierre Boilot for providing the nanoparticles and Eric Camerer for a critical reading of the manuscript.

Received: December 4, 2013
Revised: February 20, 2014
Accepted: February 21, 2014
Published: April 10, 2014

REFERENCES

Abouantoun, T.J., and MacDonald, T.J. (2009). Imatinib blocks migration and invasion of medulloblastoma cells by concurrently inhibiting activation of platelet-derived growth factor receptor and transactivation of epidermal growth factor receptor. Mol. Cancer Ther. *8*, 1137–1147.

Anastasiou, D., Poulogiannis, G., Asara, J.M., Boxer, M.B., Jiang, J.K., Shen, M., Bellinger, G., Sasaki, A.T., Locasale, J.W., Auld, D.S., et al. (2011). Inhibition of pyruvate kinase M2 by reactive oxygen species contributes to cellular antioxidant responses. Science *334*, 1278–1283.

Andrae, J., Gallini, R., and Betsholtz, C. (2008). Role of platelet-derived growth factors in physiology and medicine. Genes Dev. *22*, 1276–1312.

Banes-Berceli, A.K., Ogobi, S., Tawfik, A., Patel, B., Shirley, A., Pollock, D.M., Fulton, D., and Marrero, M.B. (2005). Endothelin-1 activation of JAK2 in vascular smooth muscle cells involves NAD(P)H oxidase-derived reactive oxygen species. Vascul. Pharmacol. *43*, 310–319.

Bedard, K., and Krause, K.H. (2007). The NOX family of ROS-generating NADPH oxidases: physiology and pathophysiology. Physiol. Rev. *87*, 245–313.

Beers, R.F., Jr., and Sizer, I.W. (1952). A spectrophotometric method for measuring the breakdown of hydrogen peroxide by catalase. J. Biol. Chem. *195*, 133–140.

Belousov, V.V., Fradkov, A.F., Lukyanov, K.A., Staroverov, D.B., Shakhbazov, K.S., Terskikh, A.V., Lukyanov, S., and Lukyanov, S. (2006). Genetically encoded fluorescent indicator for intracellular hydrogen peroxide. Nat. Methods *3*, 281–286.

Bilan, D.S., Pase, L., Joosen, L., Gorokhovatsky, A.Y., Ermakova, Y.G., Gadella, T.W.J., Grabher, C., Schultz, C., Lukyanov, S., and Belousov, V.V. (2013). HyPer-3: a genetically encoded H(2)O(2) probe with improved performance for ratiometric and fluorescence lifetime imaging. ACS Chem. Biol. *8*, 535–542.

Bouzigues, C., and Dahan, M. (2007). Transient directed motions of GABA(A) receptors in growth cones detected by a speed correlation index. Biophys. J. *92*, 654–660.

Bouzigues, C., Morel, M., Triller, A., and Dahan, M. (2007). Asymmetric redistribution of GABA receptors during GABA gradient sensing by nerve growth cones analyzed by single quantum dot imaging. Proc. Natl. Acad. Sci. USA *104*, 11251–11256.

Bouzigues, C., Holcman, D., and Dahan, M. (2010). A mechanism for the polarity formation of chemoreceptors at the growth cone membrane for gradient amplification during directional sensing. PLoS ONE *5*, e9243.

Casanova, D., Bouzigues, C., Nguyên, T.L., Ramodiharilafy, R.O., Bouzhir-Sima, L., Gacoin, T., Boilot, J.-P., Tharaux, P.-L., and Alexandrou, A. (2009). Single europium-doped nanoparticles measure temporal pattern of reactive oxygen species production inside cells. Nat. Nanotechnol. *4*, 581–585.

Chansel, D., Ciroldi, M., Vandermeersch, S., Jackson, L.F., Gomez, A.M., Henrion, D., Lee, D.C., Coffman, T.M., Richard, S., Dussaule, J.C., and Tharaux, P.L. (2006). Heparin binding EGF is necessary for vasospastic response to endothelin. FASEB J. *20*, 1936–1938.

Chen, K.C., Zhou, Y., Zhang, W., and Lou, M.F. (2007). Control of PDGF-induced reactive oxygen species (ROS) generation and signal transduction in human lens epithelial cells. Mol. Vis. *13*, 374–387.

Clempus, R.E., and Griendling, K.K. (2006). Reactive oxygen species signaling in vascular smooth muscle cells. Cardiovasc. Res. *71*, 216–225.

D'Autréaux, B., and Toledano, M.B. (2007). ROS as signalling molecules: mechanisms that generate specificity in ROS homeostasis. Nat. Rev. Mol. Cell Biol. *8*, 813–824.

Daou, G.B., and Srivastava, A.K. (2004). Reactive oxygen species mediate Endothelin-1-induced activation of ERK1/2, PKB, and Pyk2 signaling, as well as protein synthesis, in vascular smooth muscle cells. Free Radic. Biol. Med. *37*, 208–215.

de Rezende, F.F., Martins Lima, A., Niland, S., Wittig, I., Heide, H., Schröder, K., and Eble, J.A. (2012). Integrin $\alpha7\beta1$ is a redox-regulated target of hydrogen peroxide in vascular smooth muscle cell adhesion. Free Radic. Biol. Med. *53*, 521–531.

Dehmelt, L., and Bastiaens, P.I.H. (2010). Spatial organization of intracellular communication: insights from imaging. Nat. Rev. Mol. Cell Biol. *11*, 440–452.

Denu, J.M., and Tanner, K.G. (1998). Specific and reversible inactivation of protein tyrosine phosphatases by hydrogen peroxide: evidence for a sulfenic acid intermediate and implications for redox regulation. Biochemistry *37*, 5633–5642.

Dhar, K., Dhar, G., Majumder, M., Haque, I., Mehta, S., Van Veldhuizen, P.J., Banerjee, S.K., and Banerjee, S. (2010). Tumor cell-derived PDGF-B potentiates mouse mesenchymal stem cells-pericytes transition and recruitment through an interaction with NRP-1. Mol. Cancer *9*, 209.

Edidin, M., Zúñiga, M.C., and Sheetz, M.P. (1994). Truncation mutants define and locate cytoplasmic barriers to lateral mobility of membrane glycoproteins. Proc. Natl. Acad. Sci. USA *91*, 3378–3382.

Franca-Koh, J., and Devreotes, P.N. (2004). Moving forward: mechanisms of chemoattractant gradient sensing. Physiology (Bethesda) *19*, 300–308.

Fukumoto, Y., Kurita, S., Takai, Y., and Ogita, H. (2011). Role of scaffold protein afadin dilute domain-interacting protein (ADIP) in platelet-derived growth factor-induced cell movement by activating Rac protein through Vav2 protein. J. Biol. Chem. *286*, 43537–43548.

Gan, H.K., Walker, F., Burgess, A.W., Rigopoulos, A., Scott, A.M., and Johns, T.G. (2007). The epidermal growth factor receptor (EGFR) tyrosine kinase inhibitor AG1478 increases the formation of inactive untethered EGFR dimers. Implications for combination therapy with monoclonal antibody 806. J. Biol. Chem. *282*, 2840–2850.

Graves, L.M., Bornfeldt, K.E., Sidhu, J.S., Argast, G.M., Raines, E.W., Ross, R., Leslie, C.C., and Krebs, E.G. (1996). Platelet-derived growth factor stimulates protein kinase A through a mitogen-activated protein kinase-dependent pathway in human arterial smooth muscle cells. J. Biol. Chem. *271*, 505–511.

Grotendorst, G.R., Chang, T., Seppä, H.E., Kleinman, H.K., and Martin, G.R. (1982). Platelet-derived growth factor is a chemoattractant for vascular smooth muscle cells. J. Cell. Physiol. *113*, 261–266.

Heldin, C.H., and Westermark, B. (1999). Mechanism of action and in vivo role of platelet-derived growth factor. Physiol. Rev. *79*, 1283–1316.

Hellberg, C., Ostman, A., and Heldin, C.H. (2010). PDGF and vessel maturation. Recent Results Cancer Res. *180*, 103–114.

Henley, J.R., Huang, K.H., Wang, D., and Poo, M.M. (2004). Calcium mediates bidirectional growth cone turning induced by myelin-associated glycoprotein. Neuron *44*, 909–916.

Iglesias, P.A., and Devreotes, P.N. (2008). Navigating through models of chemotaxis. Curr. Opin. Cell Biol. *20*, 35–40.

Irwin, M.E., Mueller, K.L., Bohin, N., Ge, Y., and Boerner, J.L. (2011). Lipid raft localization of EGFR alters the response of cancer cells to the EGFR tyrosine kinase inhibitor gefitinib. J. Cell. Physiol. *226*, 2316–2328.

Jin, H., Heller, D.A., Kalbacova, M., Kim, J.H., Zhang, J.Q., Boghossian, A.A., Maheshri, N., and Strano, M.S. (2010). Detection of single-molecule H2O2 signalling from epidermal growth factor receptor using fluorescent single-walled carbon nanotubes. Nat. Nanotechnol. *5*, 302–309.

Kamata, H., Honda, S., Maeda, S., Chang, L., Hirata, H., and Karin, M. (2005). Reactive oxygen species promote TNFalpha-induced death and sustained JNK activation by inhibiting MAP kinase phosphatases. Cell *120*, 649–661.

Kang, S.W., Chae, H.Z., Seo, M.S., Kim, K., Baines, I.C., and Rhee, S.G. (1998). Mammalian peroxiredoxin isoforms can reduce hydrogen peroxide

generated in response to growth factors and tumor necrosis factor-alpha. J. Biol. Chem. *273*, 6297–6302.

Kim, K., Yu, M., Han, S., Oh, I., Choi, Y.J., Kim, S., Yoon, K., Jung, M., and Choe, W. (2009). Expression of human peroxiredoxin isoforms in response to cervical carcinogenesis. Oncol. Rep. *21*, 1391–1396.

Kim, J.H., Patra, C.R., Arkalgud, J.R., Boghossian, A.A., Zhang, J.Q., Han, J.H., Reuel, N.F., Ahn, J.H., Mukhopadhyay, D., and Strano, M.S. (2011). Single-molecule detection of H_2O_2 mediating angiogenic redox signaling on fluorescent single-walled carbon nanotube array. ACS Nano. *5*, 7848–7857.

Kinkhabwala, A., and Bastiaens, P.I. (2010). Spatial aspects of intracellular information processing. Curr. Opin. Genet. Dev. *20*, 31–40.

Koller, A. (2002). Signaling pathways of mechanotransduction in arteriolar endothelium and smooth muscle cells in hypertension. Microcirculation *9*, 277–294.

Kovalenko, M., Gazit, A., Böhmer, A., Rorsman, C., Rönnstrand, L., Heldin, C.H., Waltenberger, J., Böhmer, F.D., and Levitzki, A. (1994). Selective platelet-derived growth factor receptor kinase blockers reverse sis-transformation. Cancer Res. *54*, 6106–6114.

Kreuzer, J., Viedt, C., Brandes, R.P., Seeger, F., Rosenkranz, A.S., Sauer, H., Babich, A., Nürnberg, B., Kather, H., and Krieger-Brauer, H.I. (2003). Platelet-derived growth factor activates production of reactive oxygen species by NAD(P)H oxidase in smooth muscle cells through Gi1,2. FASEB J. *17*, 38–40.

Kusumi, A., Nakada, C., Ritchie, K., Murase, K., Suzuki, K., Murakoshi, H., Kasai, R.S., Kondo, J., and Fujiwara, T. (2005). Paradigm shift of the plasma membrane concept from the two-dimensional continuum fluid to the partitioned fluid: high-speed single-molecule tracking of membrane molecules. Annu. Rev. Biophys. Biomol. Struct. *34*, 351–378.

Lin, L.J., Grimme, J.M., Sun, J., Lu, S., Gai, L., Cropek, D.M., and Wang, Y. (2013). The antagonistic roles of PDGF and integrin $\alpha v\beta 3$ in regulating ROS production at focal adhesions. Biomaterials *34*, 3807–3815.

Lippert, A.R., Van de Bittner, G.C., and Chang, C.J. (2011). Boronate oxidation as a bioorthogonal reaction approach for studying the chemistry of hydrogen peroxide in living systems. Acc. Chem. Res. *44*, 793–804.

Ljungquist-Höddelius, P., Lirvall, M., Wasteson, A., and Magnusson, K.E. (1991). Lateral diffusion of PDGF beta-receptors in human fibroblasts. Biosci. Rep. *11*, 43–52.

Marco, E., Wedlich-Soldner, R., Li, R., Altschuler, S.J., and Wu, L.F. (2007). Endocytosis optimizes the dynamic localization of membrane proteins that regulate cortical polarity. Cell *129*, 411–422.

Mayer, T.J., Frauenhoffer, E.E., and Meyers, A.C. (2000). Expression of epidermal growth factor and platelet-derived growth factor receptors during cervical carcinogenesis. In Vitro Cell. Dev. Biol. Anim. *36*, 667–676.

Meng, T.C., Fukada, T., and Tonks, N.K. (2002). Reversible oxidation and inactivation of protein tyrosine phosphatases in vivo. Mol. Cell *9*, 387–399.

Myllärniemi, M., Frösen, J., Calderón Ramirez, L.G., Buchdunger, E., Lemström, K., and Häyry, P. (1999). Selective tyrosine kinase inhibitor for the platelet-derived growth factor receptor in vitro inhibits smooth muscle cell proliferation after reinjury of arterial intima in vivo. Cardiovasc. Drugs Ther. *13*, 159–168.

Okada, A., Yaguchi, T., Kanno, T., Gotoh, A., Nakano, T., and Nishizaki, T. (2012). PDGF-D/PDGF-$\beta\beta$ receptor-regulated chemotaxis of malignant mesothelioma cells. Cell. Physiol. Biochem. *29*, 241–250.

Owusu-Ansah, E., and Banerjee, U. (2009). Reactive oxygen species prime Drosophila haematopoietic progenitors for differentiation. Nature *461*, 537–541.

Pahara, J., Shi, H., Chen, X., and Wang, Z. (2010). Dimerization drives PDGF receptor endocytosis through a C-terminal hydrophobic motif shared by EGF receptor. Exp. Cell Res. *316*, 2237–2250.

Postma, M., and Van Haastert, P.J. (2001). A diffusion-translocation model for gradient sensing by chemotactic cells. Biophys. J. *81*, 1314–1323.

Rhee, S.G. (2006). Cell signaling. H2O2, a necessary evil for cell signaling. Science *312*, 1882–1883.

Saito, Y., Haendeler, J., Hojo, Y., Yamamoto, K., and Berk, B.C. (2001). Receptor heterodimerization: essential mechanism for platelet-derived growth factor-induced epidermal growth factor receptor transactivation. Mol. Cell. Biol. *21*, 6387–6394.

San Martín, A., and Griendling, K.K. (2010). Redox control of vascular smooth muscle migration. Antioxid. Redox Signal. *12*, 625–640.

Seppä, H.E., Grotendorst, G.R., Seppä, S., Schiffmann, E., and Martin, G.R. (1982). Platelet-derived growth factor in chemotactic for fibroblasts. J. Cell Biol. *92*, 584–588.

Servant, G., Weiner, O.D., Herzmark, P., Balla, T., Sedat, J.W., and Bourne, H.R. (2000). Polarization of chemoattractant receptor signaling during neutrophil chemotaxis. Science *287*, 1037–1040.

Sines, T., Granot-Attas, S., Weisman-Welcher, S., and Elson, A. (2007). Association of tyrosine phosphatase epsilon with microtubules inhibits phosphatase activity and is regulated by the epidermal growth factor receptor. Mol. Cell. Biol. *27*, 7102–7112.

Slaughter, B.D., Das, A., Schwartz, J.W., Rubinstein, B., and Li, R. (2009). Dual modes of cdc42 recycling fine-tune polarized morphogenesis. Dev. Cell *17*, 823–835.

Sundaresan, M., Yu, Z.X., Ferrans, V.J., Irani, K., and Finkel, T. (1995). Requirement for generation of H_2O_2 for platelet-derived growth factor signal transduction. Science *270*, 296–299.

Turner, N.C., Dollery, C.T., and Williams, A.J. (1989). Endothelin-1-induced contractions of vascular and tracheal smooth muscle: effects of nicardipine and BRL 34915. J. Cardiovasc. Pharmacol. *13* (*Suppl 5*), S180–S182.

Ueda, M., Sako, Y., Tanaka, T., Devreotes, P., and Yanagida, T. (2001). Single-molecule analysis of chemotactic signaling in Dictyostelium cells. Science *294*, 864–867.

Weima, S.M., van Rooijen, M.A., Mummery, C.L., Feyen, A., de Laat, S.W., and van Zoelen, E.J. (1990). Identification of the type-B receptor for platelet-derived growth factor in human embryonal carcinoma cells. Exp. Cell Res. *186*, 324–331.

Wiley, K.E., and Davenport, A.P. (2004). Endothelin receptor pharmacology and function in the mouse: comparison with rat and man. J. Cardiovasc. Pharmacol. *44* (*Suppl 1*), S4–S6.

Woo, S.-Y., Kim, D.-H., Jun, C.-B., Kim, Y.-M., Haar, E.V., Lee, S.-I., Hegg, J.W., Bandhakavi, S., Griffin, T.J., and Kim, D.-H. (2007). PRR5, a novel component of mTOR complex 2, regulates platelet-derived growth factor receptor beta expression and signaling. J. Biol. Chem. *282*, 25604–25612.

Woo, H.A., Yim, S.H., Shin, D.H., Kang, D., Yu, D.-Y., and Rhee, S.G. (2010). Inactivation of peroxiredoxin I by phosphorylation allows localized H(2)O(2) accumulation for cell signaling. Cell *140*, 517–528.

Zuo, L., Ushio-Fukai, M., Ikeda, S., Hilenski, L., Patrushev, N., and Alexander, R.W. (2005). Caveolin-1 is essential for activation of Rac1 and NAD(P)H oxidase after angiotensin II type 1 receptor stimulation in vascular smooth muscle cells: role in redox signaling and vascular hypertrophy. Arterioscler. Thromb. Vasc. Biol. *25*, 1824–1830.

